2009 American Control Conference
Hyatt Regency Riverfront, St. Louis, MO, USA
June 10-12, 2009

Multiscale modeling of atomic layer deposition processes

Vivek Dwivedi and Raymond A. Adomaitis

***Abstract*— A multiscale simulator for alumina film growth inside a nanoporous material during an atomic layer deposition process is developed. The model combines a continuum description at the macroscopic level of precursor gas transport inside a nanopore during exposure to each of the two precursor species (trimethyaluminum and water) with a Monte Carlo simulation of the film growth on the microscopic scale. Simulation results are presented for both the Monte Carlo simulation and for the multiscale system, the latter illustrating how nonuniform deposition along the nanopore can occur when insufficient precursor exposure levels are used.**

I. INTRODUCTION

Atomic Layer Deposition (ALD) is a thin film deposition process in which the growth surface is exposed to reactive precursor gases in an alternating fashion (Fig. 1). A characteristic of the surface adsorption and reaction mechanisms is that they are normally self limiting, allowing for atomically accurate control of film thickness and uniform deposition over complex surface topologies.

ALD is an important unit operation in manufacturing nanoscale devices. ALD, in fact, is the key enabling technology in Intel's current 45nm transistor manufacturing process to deposit the HfO_2 gate oxide [2]. Another example of ALD use is the production of the nanolaminates for large-scale flat-panel electroluminescence displays [12]. ALD has even greater potential in future manufacturing and research applications, such as in the deposition of gate dielectrics for carbon nanotube transitors [10], nanoelectrodes for studying single molecules [9], and other nanoparticle [11] and nanolaminate [6] applications.

ALD is an inherently dynamic process characterized by multiple time scales: a faster time scale corresponding to the molecular events taking place during each exposure cycle, and the slower *overall* nucleation and steady growth[1] time scales [8]. Likewise, multiple length scales are found in these systems where macroscopic length scales (100's of μm) correspond to gas phase transport effects, and microscopic scales characterize the atomistic nature of the film growth. An approach to coupling modeling elements across these scales to simulate ALD growth of alumina films inside nanopores of high aspect ratio is the topic of this paper.

R. A. Adomaitis is with Faculty of Department of Chemical and Biomolecular Engineering and Institute for Systems Research, University of Maryland, College Park, MD, 20742, USA. adomaiti@umd.edu

V. Dwivedi is a PhD student in Department of Chemical and Biomolecular Engineering and Institute for Systems Research, University of Maryland, College Park, MD, 20742, USA. vivek.h.dwivedi@nasa.gov

[1]The cycle-integrated growth rate defining the total film thickness added during each exposure cycle.

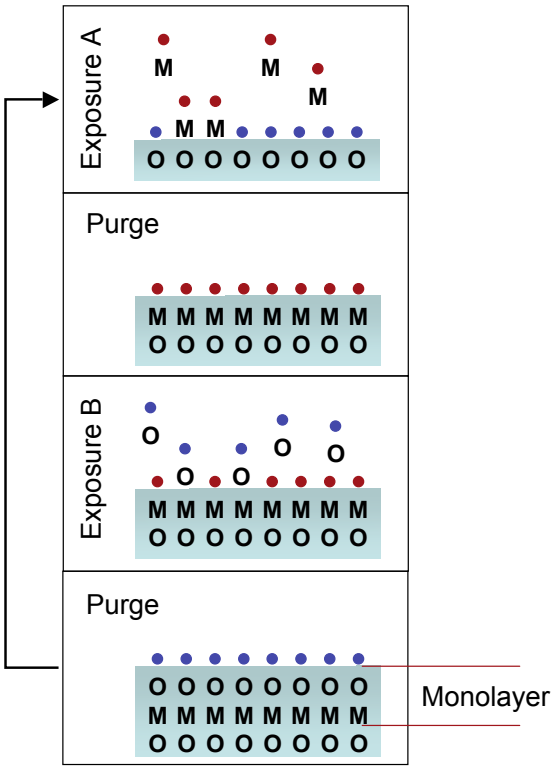

Fig. 1. *Substeps of a full ALD cycle. In this process a metal oxide film is being deposited; the metal (M) is deposited in half-cycle A, and the oxygen precursor is supplied during half-step B.*

A. Al_2O_3 ALD

We consider Al_2O_3 ALD, one of the most widely studied ALD systems (see, e.g., [3], [14]) and the material system used to modify nanostructured catalytic membrane pore size [5], [13]. Amorphous Al_2O_3 films can be grown from alternate exposures of the growth surface to TMA ($Al(CH_3)_3$) and water.

Represented in Fig. 2 are the reactions that take place under ideal ALD conditions during exposure of the growth surface to sufficient dosages of TMA and then to water. In reality, exposure of the growth surface to each of the precursors does not guarantee complete conversion of the surface groups and this simple picture cannot describe the other potential reactions that can take place on the growth surface, nor can it describe the amorphous structure of the film. Because of the importance of positions of each surface species with respect to its neighbors, a simulation approach that accounts for the spatially dependent nature of the reactions was developed and is described next.

978-1-4244-4524-0/09/$25.00 ©2009 AACC

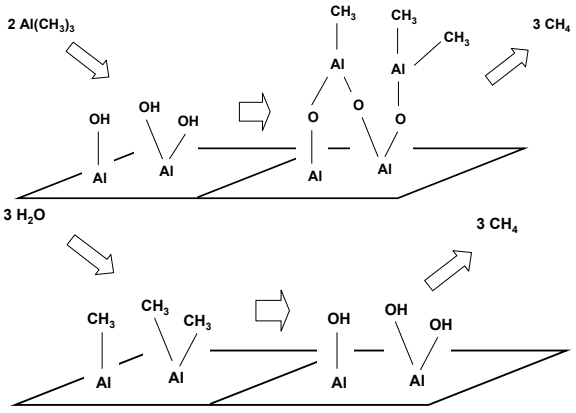

Fig. 2. *Ideal Al_2O_3 ALD, after [3], showing the reactions resulting from exposure to TMA (top) and then to water (bottom)*

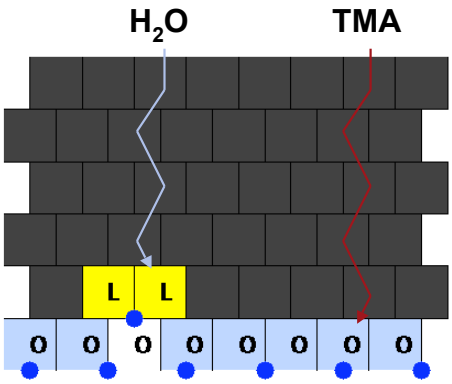

Fig. 3. *ALD film lattice illustrating the growth surface at bottom and the transport of water and TMA precursor species in the region immediately above the surface. Note that the water molecules require a path only one lattice site in width to travel downwards to react with the methyl group ligand (L) while the larger TMA molecules require at least two horizontally adjacent sites to travel downwards to react with the hydroxyl group (O) at the growth surface.*

II. FILM GROWTH MODEL

The ALD process is inherently dynamic, with the growth surface exposed to a time dependent precursor partial-pressure profile that depends on gas-phase transport and surface reactions on the scale of the overall deposition system. In our ALD reaction simulation approach, we focus on a microscopic region of the growth surface and discretize this region into a two dimensional grid of lattice sites, one dimension representing spatial position along the growth surface (with periodic boundary conditions), and the other the depth of the deposited film (Fig. 3). Each of the lattice sites will contain a surface group or bond structure potentially capable of undergoing a reaction, a deposited film species, or will be empty.

A. The Al_2O_3 lattice

The density of bulk Al_2O_3 is reported to be between 3.5 and 4g/cm^3; given its molecular weight of 101.98g/mol, we can compute an aluminum atom number density of approximately 41 Al atoms/nm^3 and 62 O atoms/nm^3. If we consider the basic molecular unit of an amorphous alumina film to be an $Al_{2/3}O$ unit, the volume of this unit is 0.016nm^3 or a square box with sides approximately 0.25nm in length.

1) Species occupying the lattice sites: Give the lattice box size of 0.25nm, we now consider the chemical species that occupy the sites. As computed, each site can contain one $Al_{2/3}O$, and so an Al_2O_3 molecule occupies three adjacent sites. The van der Walls radius of the methyl group CH_3 is 0.2nm [14]; this corresponds to a cross-sectional area of 0.1257nm meaning the CH_3 ligand is larger than our lattice box size[2]. This will limit the density of the methyl groups across the growth surface and the steric hindrance effects will be accounted for in the TMA surface reactions. The hydroxyl group OH fits easily within each lattice site; sites on the growth surface may also contain the Al-O bonds corresponding to oxygen bridges that may undergo dissociation reactions with either precursor species.

2) Growth per cycle: Experimentally measured growth-per-cycle (GPC) rates are typically 0.11nm per ALD processing cycle. What is important to note is that these measurements are normally made by measuring a change in mass during the deposition process, not by direct measurement of the growth surface. Therefore, if M is the number of lattice sites in the horizontal direction and Δn_a is the number of aluminum atoms deposited during a deposition cycle,

$$GPG = (0.25nm)\frac{3\Delta n_a}{2M}. \quad (1)$$

B. Microscopic gas-phase transport

ALD processes operate a sufficiently low pressures and temperatures above 300K, and so the kinetic theory of gases provides a very good approximation to the precursor gas behavior. From the idealized gas descriptions, we can compute the surface collision rate as a function of precursor partial pressure; that information, plus the total exposure time defines the number of precursor gas collisions that occur at the growth surface. In this study, we assume the water and TMA gas species travel downwards through the lattice to the growth surface by paths shown in Fig. 3. Because the water molecule size is comparable to the lattice site size, we assume if follows a single column downward until it reaches the substrate unless a reaction takes place within the film. The TMA precursor's much larger size[3] requires two adjacent lattice columns; its downward progress is stopped at the growth surface, when the potential for a surface reaction is checked.

C. The reactions

In [3], FTIR spectroscopy was used to examine the surface reactions of an Al_2O_3 process in real-time. From the observations, the key reactions between the TMA and water precursors and the growth surface were identified. The three

[2][14] further states that the greatest density with which methyl groups can pack the growth surface is 7.2 per nm^2 and typical saturation conditions are 70-80% of that.

[3]TMA can form a dimer, but it is found in its monomer form at the temperature and pressures we consider.

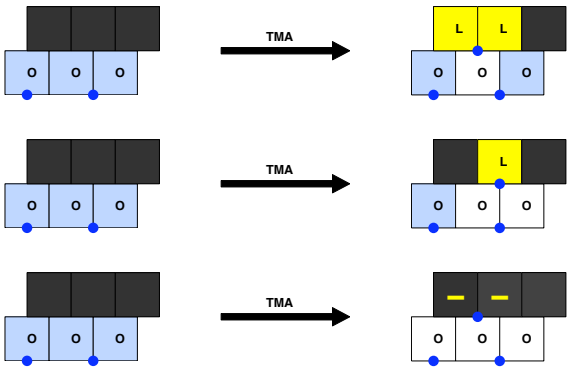

Fig. 4. *TMA reaction with a single OH group (top); two OH groups (middle), and three OH groups (bottom).*

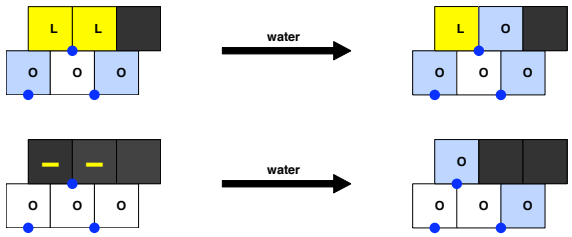

Fig. 5. *Water reactions.*

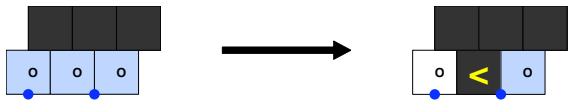

Fig. 6. *(Spontaneous) dehydroxylation reaction.*

potential reactions involving TMA, two involving water, and one spontaneous dehydroxylation reaction are described next.

1) TMA reactions: In Fig. 4, we see on the top left a fully hydroxilated growth surface; the OH groups occupy the (light blue) lattice sites at the lower level, and the upper level is empty. The Al atoms are denoted by the filled dark blue circles below the hydoxyl groups; note that an Al atom is bound to a single OH group when it is centered below a lattice site, and it is bound to two when it is located between two lattice sites. In the first reaction, a TMA molecule reacts with a single surface OH group, releasing one methane molecule and leaving two CH_3 ligands (yellow sites containing the letter L) bound to the newly-deposited Al atom. Note that the hydroxyl group looses an H atom in the process, changing the site color from blue to white. This chemisorbed surface species can undergo a second reaction with a neighboring surface OH leaving one surface CH_3 which can undergo yet another reaction with an available surface OH, leaving a surface Al bound to three O atoms (these oxygen bridge structures are denoted by the (-) symbols in Fig. 4, bottom reaction. It is argued in [3] that the reaction of TMA with three neighboring OH groups is favored over the other two partial reactions, and so our reaction model will assume this reaction sequence goes to completion whenever sufficient surface OH groups are present.

2) Water reactions: The two major reactions involving water are shown in Fig. 5. By far, the most important of this is the reaction of water with a surface CH_3 species, releasing a methane molecule and generating a new surface OH group (Fig. 5, top). Water can also participate in the dissociative breaking of a surface oxygen bridge, resulting in two new surface OH groups (Fig. 5, bottom).

3) Dehydroxylation reaction: It is argued in [3] and [15] that higher growth temperatures result in decreased growth rate due to the dehydroxilation reaction that can take place between neighboring surface OH groups. This reaction is illustrated in Fig. 6, where the reaction between two adjacent OH surface groups results in the formation of one water vapor molecule; the lattice site from which the oxygen is removed is replaced with an arrowhead pointing to the surface oxygen atom making up the resulting oxygen bridge. All of the simulation studies considered in this work take place in the lower temperature range of Al_2O_3 ALD and so this reaction will not be considered further.

D. Film growth simulator predictions

Representative results of our microscopic simulator are shown in the form of a surface region snapshot in Fig. 7. In this figure, the initial condition of the growth surface is a fully hydroxilated Al_2O_3. After 100 cycles, a substantial film has been produced with an irregular structure consistent with amorphous alumina.

As discussed earlier, the mean incorporation rate of aluminum can be used to determine the growth rate after each cycle (equation 1); plotting the dynamics of film growth in terms of GPC (Fig. 8), we see a relatively steady film growth rate after the initial growth period. The observed steady growth rate of slightly greater that 0.1nm/deposition cycle is consistent with experimental observations, as is the decay of the initially rapid growth rate on the fully hydroxilized substrate [3]. Further validation of the model predictions is currently underway.

III. MULTISCALE SIMULATION

Nanostructured membranes and nanostructured catalytic membranes (NCM), have numerous chemical reaction, storage, and separation applications. They can be created using an anodic aluminum oxide scaffold, with pore sizes and surface properties subsequently modified to high precision using an ALD process. We now focus on developing a multiscale (continuum transport at the reactor scale, lattice Monte Carlo simulation of the film growth process at the atomistic scale) simulator of the ALD process taking place within these nanoporous materials.

We consider a simplified description of gas phase transport and surface reaction of the TMA and water precursors within a $250\mu m$ long nanopore (Fig. 9), where gas phase transport

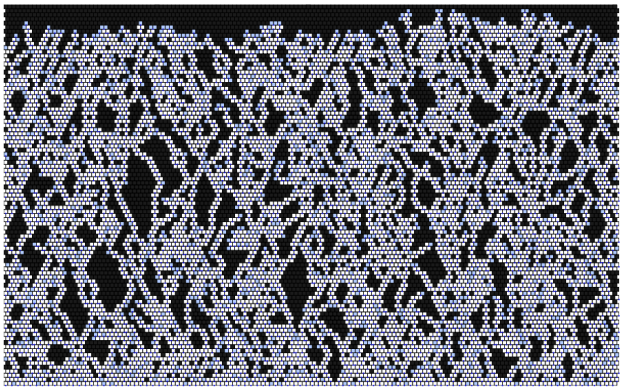

Fig. 7. *Amorphous ALD Al_2O_3 produced after 100 deposition cycles.*

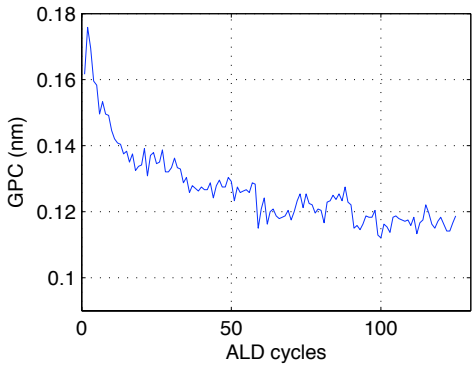

Fig. 8. *Growth per cycle (GPC) for 125 ALD cycles and 900 horizontal lattice sites.*

is described by Knudsen diffusion[4]:

$$\frac{\partial p_A}{\partial t} = \frac{2}{3} r(s) \sqrt{\frac{8RT}{\pi M}} \pi r^2(s) \frac{\partial p_A}{\partial s} - 2\alpha\pi r(s) C_A(p_A) \quad (2)$$

where $p_A(s,t)$ is the partial pressure of TMA inside the nanopore, $r(s)$ is the local pore radius, $0 \leq s \leq 1$ is the dimensionless axial coordinate of the pore, C_A is the local consumption rate of the TMA precursor by the surface reaction, and α is the pore aspect ratio. A similar modeling equation exists for the water partial pressure. Because ALD is a cyclic process, one simplification we use is to average (2) over the TMA exposure (half) cycle, giving a *local precursor dosage* $\delta_A(s)$ for the TMA precursor (δ_W for water) as a function of spatial position along the pore:

$$\delta_A(s) = \int_0^{\tau_A} p_A(s,t) dt$$

and

$$c_A(\delta_A(s)) = \int_0^{\tau_A} C_A(p_A(s,t)) dt.$$

The resulting boundary value problem, subject to a specified

[4]See the work on tungsten CVD in a trench by Cale and co-workers, e.g., [16] for justification of this modeling approach. IN our system we find the Knudsen number $Kn \approx 1000$, clearly indicating this mode of diffusive transport.

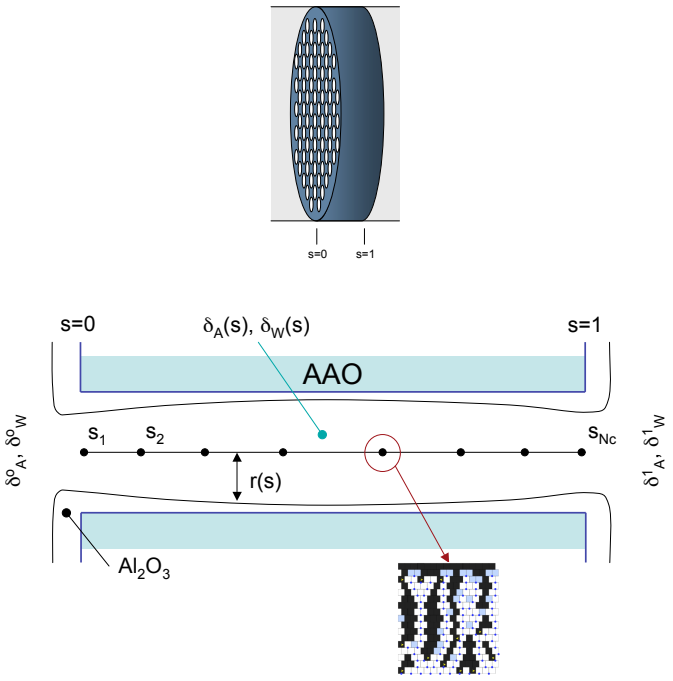

Fig. 9. *Nanoporous film (top) and closeup of an individual pore's geometry (bottom) illustrating the macroscopic scale s over which which the cycle-averaged TMA and water partial pressures (δ_A and δ_W, respectively) are defined. Individual MC models are evaluated at the collocation points s_n.*

exposure level at each end of the pore ($s = 0, 1$) is given by:

$$\frac{d}{ds}\frac{2}{3} r(s) \sqrt{\frac{8RT}{\pi M}} \pi r^2(s) \frac{d\delta_A}{ds} - 2\alpha\pi r(s) C_A(\delta_A) = 0$$

subject to the pore entrance BCs

$$\delta_A(0) = \delta_A^o, \quad \delta_A(1) = \delta_A^1$$

and the update to the deposition thickness profile after each full deposition cycle:

$$r^n(s) = r^{n-1}(s) + GPC^{n-1}(s) \quad \text{with } n = \text{cycle number.}$$

The boundary value problems are discretized using orthogonal collocation [1]; note that the dose-averaged rate terms c_A must be evaluated at each collocation point using the lattice Monte Carlo simulators, resulting in a numerical problem combining a pore-scale continuum description of transport in the nanopore and a sequence of microscopic simulator elements (Fig. 9) for film growth.

The macroscopic variables for the system are the half-cycle averaged precursor partial pressures $\delta_A(s)$ and $\delta_W(s)$, and because of the stochastic nature of the microscopic models that are used to determine c_A and c_W, the spatially discretized modeling equations cannot be written explicitly. Instead, the current solution profile estimates $\delta_A(s)$ and $\delta_W(s)$ are used to determine the number of MC simulation steps in a sequence of microscopic simulations, each located at one of the collocation points, determining the local reactant consumption rate $c_A(s_n)$ and $c_W(s_n)$. The residuals of the modeling equations thus are determined; during each microscopic simulation, we also compute the sensitivity of each

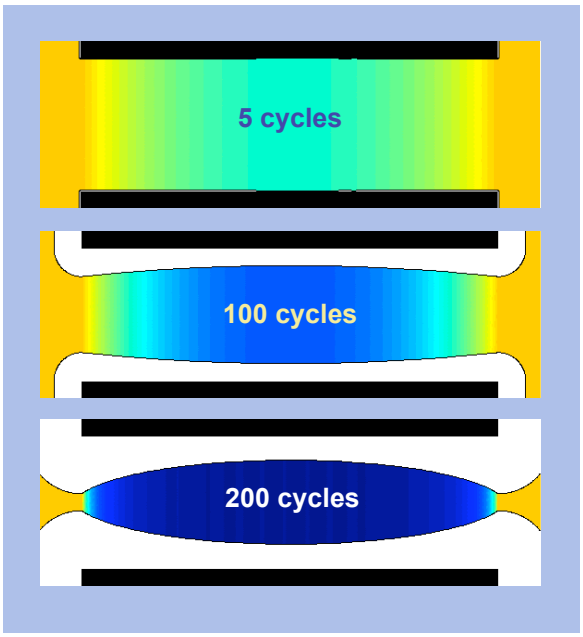

Fig. 10. *Symmetric pore mouth boundary conditions. Deposited pore film thickness is shown in white, original pore outline in black, along with the gas phase TMA time-averaged partial pressure. Profiles correspond to cycle 5 (top), 100 (middle), and 200 (bottom).*

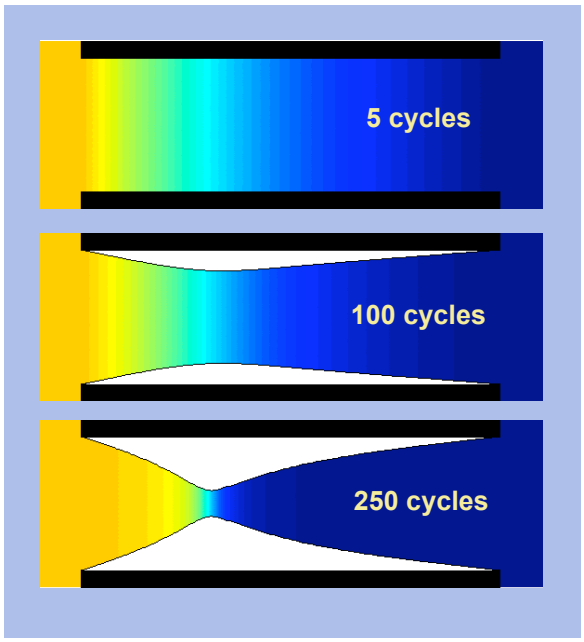

Fig. 11. *Asymmetric boundary conditions.Profiles correspond to cycle 5 (top), 100 (middle), and 250 (bottom).*

$c_A(s_n)$ and $c_W(s_n)$ to $\delta_A(s_n)$ and $\delta_W(s_n)$, respectively. These sensitivities, along with the collocation discretization arrays for the differential terms in the macroscopic modeling equations, define the elements of the Jacobian array needed for the Newton-Raphson procedure used to iteratively solve the macroscopic modeling equations.

The entire numerical approach is implemented using object-oriented elements of MATLAB, and representative results are shown in Figs. 10 and 11. In this simulation, the nanopore initially has a uniform radius of 100Å and the boundary condition precursor exposure levels for the symmetric case shown in Fig. 10 are $\delta_A^o = \delta_A^1 = 2$ and $\delta_W^o = \delta_W^1 = 3$, levels that are just over the exposure needed for ideal ALD growth with no mass transfer limitations. The TMA and water precursors diffuse into the open ends of the nanopore during each exposure step, and a portion is adsorbed onto the pore walls. Early in the deposition process (e.g., after cycle 5), we observe only a small amount of precursor depletion in the innermost regions of the pore. However, the depletion effects grow with increasing number of deposition cycles, leading to preferential deposition near the pore mouths, further accelerating the development of the cycle-averaged precursor partial pressure $\delta_A(s)$ gradients. The simulations were performed for a total of 200 ALD cycles, after which the pore mouths essentially close, preventing further deposition within the pore. This example illustrates the potential for our numerical methods to capture the correct reaction and transport phenomena of the ALD process.

It is interesting to compare the previous case to the results shown in Fig. 11. These simulations correspond to the asymmetric boundary condition case $\delta_A^o = 2$, $\delta_A^1 = 0$ and $\delta_W^o = 0$, $\delta_W^1 = 3$. Exposing the nanomembrane to the precursors in this fashion results in a deposition profile that grows from the center outwards, illustrating the potential for controlling the uniformity by manipulating the pore mouth boundary conditions.

IV. CONCLUSIONS

A multiscale simulator for the atomic layer deposition of alumina inside a nanoporous material was presented that incorporated two major numerical ideas novel to our approach:

- The spatially distributed and time-dependent problem was simplified by considering the half-cycle averaged equations; this also simplified the microscopic simulations because kinetic (dynamic) Monte Carlo simulations were not required;
- Because the spatially distributed microscopic simulators are not correlated, the sensitivity of each microscopic model's prediction of local precursor consumption rate depends only on local, cycle-averaged precursor exposure levels. This observation greatly simplifies construction of the Jacobian array because the off-diagonal elements correspond only to macroscopic-scale modeling terms (the collocation discretiztion arrays).

Combined, these two important numerical simplifications results in a computationally efficient simulator, useful for exploring factors that give rise to nonuniformities in pore size modification by ALD processes. A more systematic study of simulator predictions is underway.

V. ACKNOWLEDGMENTS

The authors acknowledges the support of the National Science Foundation through grant CTS-0554045 and reviewers' comments.

REFERENCES

[1] Adomaitis, R. A., Objects for MWR, *Computers & Chem. Engng* **26** (2002) 981-998.

[2] Bohr, M. T. R. S. Chau, T. Ghani, and K. Mistry, The high-k solution, *IEEE Spectrum* Oct. 2007.

[3] Dillon, A. C., A. W. Ott, J. D. Way, and S. M. George, Surface chemistry of Al_2O_3 using $Al(CH_3)_3$ and H_2O in a binary reaction sequence, *Surf. Sci* **322** (1995) 230-242.

[4] Dwivedi, V. and R. A. Adomaitis, Lattice Monte Carlo simulation of amorphous alumina growth during atomic layer deposition, *manuscript in preparation* (2008).

[5] Elam, J. W., G. Xiong, C. Y. Han, H. H. Wang, J. P. Birrell, U. Welp, J. N. Hryn, M. J. Pellin, T. F. Baumann, J. F. Poco, and J. H. Satcher, Jr., Atomic layer deposition for the conformal coating of nanoporous materials, *J. Nanomaterials* (2006) 1-5.

[6] Elam, J. M., Z. A. Sechrist and S. M. George, ZnO/Al_2O_3 nanolaminates fabricated by atomic layer deposition: growth and surface roughness measurements, *Thin Solid Films* **414** 43-55 (2002).

[7] Fichthorn, K. A. and W. H. Weinberg, Theoretical foundation of dynamic Monte Carlo simulations, *J. Chem. Phys.* **95** (1991) 1090.

[8] Granneman, E., P. Fischer, D. Pierreux, H. Terhorst, P. Zagwijn, Batch ALD: Characteristics, comparison with single wafer ALD, and examples, *Surf. Coatings Tech.* **201** 8899-8907 (2007).

[9] Gupta, R. and B. G. Willis, Nanometer spaced electrodes using selective area atomic layer deposition, *Appl. Phys. Lett.* **90** (2007) 253102.

[10] Javey, A. H. Kim, M. Brink, Q. Wang, A. Ural, J. Guo, P. McINtyre, P. McEuen, M. Lundstrom, and H. Dai, High-k dielectrics for advanced carbon-nanopore transistors and logic gates, *Nature Mater.* **1** 241-246 (2002).

[11] King, D. M., J. A. Spencer II, X. liang, L. F. Hakim, and A. W. Weimer, Atomic layer deposition on particles using a fluidized bed reactor with in situ mass spectrometry, *Surf. Coatings Tech.* **201** 9163-9171 (2007).

[12] A history of electroluminescent displays http://www.indiana.edu/˜hightech/fpd/papers/ELDs.html

[13] Pellin, M. J., P. C. Stair, G. Xiong, J. W. Elam, J. Birrell, L. Curtiss, S. M. George, C. Y. Han, L. Iton, H.Kung, M. Kung, and H.-H. Wang, Mesoporous catalytic membranes: Synthetic control of pore size and wall composition *Cat. Lett.* **102** (2005) 127-130.

[14] Puurunen, R. L., Surface chemistry of atomic later deposition: A case study of the trimethylaluminum/water system, *Appl. Phys. Rev.* **97** 121301 (2005).

[15] Puurunen, R. L., Correlation between growth-per-cycle and the surface hydroxyl group concentration in the atomic layer deposition of aluminum oxide from trimethylaluminum and water, *Appl. Surf. Sci.*. **245** 6-10 (2005).

[16] Song, L., S. Shen, K. S. Tsakalis, P. E. Crouch, and T. S. Cale, Optimal control for increasing throughput in low pressure chemical vapor deposition, *Proc. 35th CDC*, Dec. 1996.